RESEARCH PAPER

Aspect-dependent efficient multipath ghost suppression in TWRI with sparse reconstruction

ALI HUSSEIN MUQAIBEL[1], ABDI TALIB ABDALLA[2], MOHAMMAD TAMIM ALKHODARY[1] AND SUHAIL AL-DHARRAB[1]

In through-the-wall radar imaging, multipath propagation can create ghost targets, which can adversely affect the image reconstruction process. However, unlike genuine targets, ghost positions are aspect-dependent, which means their position changes with the transceiver location. This paper proposes efficient ghost suppression methods exploiting aspect dependence feature under compressive sensing framework. This paper proposes a generalized signal model that accommodates for the reflections of the front-wall and target-to-target interactions, making the scheme more practical, yet the knowledge of the location of reflecting geometry is not a requirement as in most of the recent literatures. In addition, the sensing matrix is greatly reduced making the methods more attractive. Moreover, this paper investigates the influence of array configurations by examining two antenna array configurations: multimonostatic, and single-view bistatic configurations. Results based on synthesized data and real experiment show that the proposed method can greatly suppress multipath ghosts and hence increase signal-to-clutter ratio.

I. INTRODUCTION

The objective of through-the-wall radar imaging (TWRI) is to obtain high-resolution images of obscured areas using electromagnetic (EM) waves. TWRI is useful in determining interior structures of buildings, in rescuing missions in fire and earthquakes, or in undergoing law enforcing [1–6]. This technology has witnessed a tremendous growth and attracted the attention of many researchers lately.

When TWRI is used for imaging targets that are surrounded by walls, two major challenges are encountered: the effects of the front wall; and the multiple reflections from the side walls. The front wall, which is the wall standing between the targets and the radar, gives strong reflections, which weaken the signal reaching the targets behind the wall. Front wall causes multiple internal reflections, *wall reverberation*, leaving replicas of the wall and targets in the reconstructed image known as *ghosts*. The ghosts populate the scene and sometimes mask the targets especially those in the vicinity of the wall, which deteriorates the reconstruction and detection processes. Further, the front wall may reduce the receiver dynamic range and the risk of saturating and blocking the receiver [7].

The second challenge of TWRI is multipath stemming from multiple reflections of EM waves from the walls, floors, and ceilings, which also generate ghost targets [8–12]. In such scenarios, accurate target localization and tracking becomes difficult. In the literature, different techniques have been presented to suppress multipath ghosts, but their performance and/or practicability can be improved.

To obtain high-resolution images, we need wide bandwidth and large aperture. Consequently, huge amount of data need to be collected and processed [8]. Yoon and Amin [13] tackled this problem by applying compressive sensing (CS) techniques to TWRI assuming a sparse scene. As a result, only a small fraction of data is used to reconstruct the images with relatively good quality. Hence, multipath ghost suppression under CS framework inevitably becomes the preferred solution for sparse scene scenarios.

Multipath ghosts are aspect-dependent (AD), i.e. the location of the multipath ghost changes with the transceiver location. This feature has been successfully exploited to identify and suppress multipath ghosts from genuine targets [14–17]. To the best of our knowledge, no research on ghost suppression has been presented employing AD under CS framework. In [15], the authors proposed a multipath ghost suppression method exploiting AD property of the ghost using full data set. The authors modeled the ghost positions as hidden Markov chain problem. However, their method shows some

[1]Electrical Engineering Department, King Fahd University of Petroleum & Minerals, Dhahran, 31261, Saudi Arabia
[2]Electronics and Telecommunication Engineering Department, University of Dar es Salaam, Tanzania
Corresponding author:
M.T. Alkhodary
Email: mtamim@kfupm.edu.sa

inherent challenges: it requires image decomposition into N subaperture images using directional filters; and complex advanced algorithms. In [16], the authors proposed a ghost suppression method exploiting AD feature without CS. The authors formed three images using back-projection method; the first two using extreme opposite subapertures and the rest using the whole aperture. The method involves tedious searching of appropriate subapertures and shifting of antenna array in two extreme ends of the room, which can mislaid the genuine targets particularly when using directional antennas. The authors in [18] proposed a suppression technique for ghosts originated from target-to-target interactions. They suggested different array configurations with image combining strategies to combat the effect of the ghosts. However, the effect of side walls was not addressed, which is unavoidable in TWRI. In [19], the author developed multipath model, which uses AD feature in conjunction with multipath exploitation. However, the model is limited to first-order multipath from single target only. Further it requires the knowledge of the reflecting geometry. Authors in [20] proposed a new multipath ghost suppression method, which cancels multipath components from the raw data. Though the method has the capability of preserving weak targets, it increases system complexity as the method does not employ CS.

On the other hand, there are few contributions for ghost suppressions based on CS but not employing AD feature [8, 21, 22]. The authors in [8] incorporated the wall reverberation effect of the front wall, which makes their approach more practical. They inverted multipath model assuming the knowledge of the reflecting geometry, which is not always available. Further, the effect of target-to-target interactions was not addressed.

This paper proposes a new multipath ghost suppression technique, which incorporates AD feature of the ghosts under CS framework. Contrary to the conventional CS-based TWRI, a fraction of J measurements is randomly collected from a given aperture of N locations. In this work, a pair of the same fraction is collected such that the AD feature is maximized and then their corresponding images are strategically combined to suppress the effect of the ghosts. Exploiting AD feature allows to simplify the existing image reconstruction problem significantly by reducing the size of the sensing matrix and eliminating the constraint of the knowledge of reflecting geometry. In this paper, we propose a new multipath ghost suppression method in TWRI, which exploit the AD feature under CS framework. We also extend the current received signal model based on point-target assumption to a more general model, which best reflect the real TWRI scenario. The model takes into account the front-wall reflections and reverberations, the side-wall reflections and target-to-target interaction as well. In CS-based approaches, the target-to-target interaction has been ignored due to non-linear behavior. In this work, we model the target-to-target interaction as a linear component by imposing additional but justifiable assumptions.

Further, the concept of synthetic aperture radar (SAR) is used to form large aperture, which can be achieved via mechanical scanning, or phased arrays. In the former, an antenna is physically moved over the desired aperture, while in the later, several antennas are physically stacked together with phase-shifted with respect to each other [23]. For simplicity of design, we adapt the former approach in all our simulations and experiments. The paper investigates the influence of

antenna configurations toward getting unambiguous images. In this regard, two array configurations were examined: multi-monostatic and single-view bistatic configurations.

The effectiveness of the proposed method is shown using synthesized and experimental data.

The remainder of the paper is organized as follows: Section 2 introduces the TWRI signal and scene models. The effect of the front wall in the scene reconstruction and their commonly used mitigation techniques are highlighted. Proposed method is presented in Section 3 with sensing matrix design and its evaluation. Section 4 presents the results and discussion based on both synthesized and experimental data. Comparison with the recent work is tabulated herein, and Section 5 contains concluding remarks.

II. TWRI SIGNAL MODEL

Suppose there are N radar locations for the scene interrogation as in Fig. 1. At each location, M equally spaced monochromatic waves to realize an ultra-wideband (UWB) signal are transmitted and received. Similar signal was used by [21, 24, 25] in their analysis. The scene is divided into N_x pixels in cross-range by N_y pixels in downrange. The target reflectivity on a pth grid point is represented by σ_p, with $p = 0, 1, \ldots, N_x N_y - 1$ and the wall grid point reflectivity by σ_w. If R target returns and R_w wall returns are considered, the received signal, $y[m, n]$, at the nth radar location when the mth frequency, f_m, is transmitted is comprised of four main contributions: reflection from the front wall, target-to-side wall reflection, target-to-target reflection, and ambient noise, given by:

$$
\begin{aligned}
y[m, n] = &\sum_{r=0}^{R-1} \sum_{p=0}^{N_x N_y - 1} \sigma_p^{(r)} \exp\left(-j2\pi f_m t_{pn}^{(r)}\right) \\
&+ \sum_{r_w=0}^{R_w - 1} \sigma_w^{(r_w)} \exp\left(-j2\pi f_m t_w^{(r_w)}\right) \\
&+ \sum_{r=0}^{R-1} \sum_{\substack{p, q=0 \\ p \neq q}}^{N_x N_y - 1} \sigma_{pq}^{(r)} \exp\left(-j2\pi f_m t_{pqn}^{(r)}\right) + v(m, n),
\end{aligned}
$$

$$(1)$$

where $t_{pn}^{(r)}$ represents the round-trip delay between the pth target and the nth receiver due to the rth return, $t_{pnq}^{(r)}$ is the
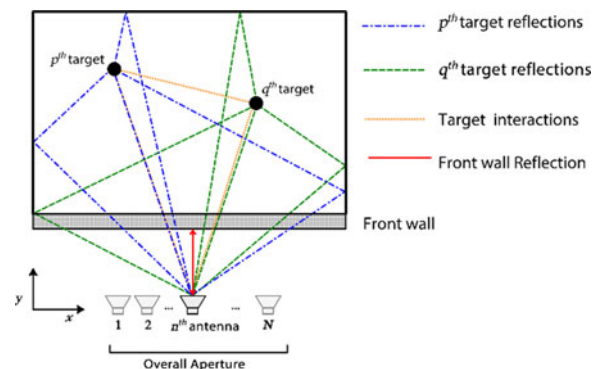

Fig. 1. TWR multipath scenario with first-order returns.

round-trip delay between p^{th} and q^{th} targets with n^{th} transceiver, and $t_w^{(r_w)}$ is the time delay of the r_w^{th} front-wall return. While $\sigma_p^{(r)}$ and $\sigma_w^{r_w}$ are the target and wall pixel reflectivity, respectively, with respect to the rth return and $v(m, n)$ is the noise sample.

Since the contribution from target interactions in (1) is non-linear, we can assume that the overall signal reflectivity due to the target interactions, $\sigma_{pq}^{(r)}$, is dictated by the second target and first target is taken as perfect reflector. Then we can replace the term $\sigma_{pq}^{(r)}$ in (1) by $\beta_p^{(r)}$.

Its corresponding matrix representation will be:

$$y = \sum_{r=0}^{R-1} \Phi^{(r)} s^{(r)} + \sum_{r_w=0}^{R_w-1} \Phi_w^{(r)} s_w^{(r)} + \sum_{r=0}^{R-1} \sum_{\substack{p,q=0 \\ p \neq q}}^{N_x N_y - 1} \Psi_q^{(r)} s_q^{(r)} + v, \quad (2)$$

where $s^{(r)}$, $s_q^{(r)}$, and $s_w^{(r_w)} \in C^{N_x N_y \times 1}$, with $r = 0, 1, \ldots R - 1$ and $r_w = 0, 1, \ldots R_w - 1$ represents the vectors of reflectivities, $\sigma_p^{(r)}$, $\beta_q^{(r)}$, and $\sigma_w^{r_w}$, respectively. The entries of the matrices $\Phi^{(r)}$, $\Phi_w^{(r)}$, and $\Psi_q^{(r)} \in C^{MN \times N_x N_y}$ are defined as:

$$\left[\Phi^{(r)}\right]_{ip} = \exp\left(-j2\pi f_m t_{pn}^{(r)}\right), \quad \left[\Psi_q^{(r)}\right]_{ip}$$
$$= \exp\left(-j2\pi f_m t_{pnq}^{(r)}\right), \quad \left[\Phi_w^{(r)}\right]_{ip} \quad (3)$$
$$= \exp\left(-j2\pi f_m t_w^{(r)}\right)$$

$$m = i \bmod M, \quad n = \frac{i}{M}, \quad i = 0, 1, 2 \ldots MN - 1.$$

In TWRI, only first-order returns (involving single reflection) have significant effects. Returns involving multiple reflections will either be very weak due to strong attenuation when interacting with walls or their corresponding ghosts will reside outside the area of interest due to elongated time delays [26]. Therefore, they are not considered in this work.

To correctly localize the targets during image reconstruction process, time delay caused by the front-wall reverberation needs to be properly taken into account, otherwise the target will be erroneously reconstructed.

A) Front-wall reverberation model

As the signal propagates through the front wall, part of it traverse and undergoes wall ringing or reverberation [8, 27]. As a result, multipath ghosts are generated in the reconstructed image that are equally spaced in the radial direction from the array with exponentially reducing intensity [8]. The wall reflections on the other hand, can be dealt with using available wall mitigation techniques [28–30].

The distance between the target and the array element in cross-range direction, Δx, in Fig. 2 can be expressed as:

$$\Delta x = (\Delta y - d) \tan \theta_{air} + d(1 + 2k) \tan \theta_{wall}, \quad (4)$$

where Δy is the distance between the target and the array element in downrange direction, θ_{air} and θ_{wall}, respectively, stand for the angles in the air and in the wall medium, d_f is the standoff distance, d represents the thickness of the front wall and integer k is the number of wall reverberations. The two angles are related by famous Snell's law.

The one-way time delay that a given return will undergo due to k wall reverberations will be [31]:

$$\tau(\Delta x, \ \Delta y, \ k) = \frac{(\Delta y - d)}{c \cos \theta_{air}} + \frac{d\sqrt{\varepsilon_r}(1 + 2k)}{c \cos \theta_{wall}}, \quad (5)$$

where c is the speed of EM wave in free space and ε_r represents the relative permittivity of the front wall. As the signal gets attenuated when it reflects within the wall, only few reverberations will be noticeable.

B) Front-wall mitigation under CS framework

Without an effective removal of the front-wall clutter, the targets hardly will be detected. For moving targets scenario, the wall effect can be alleviated by subtracting data acquired at different times. Though, this is not possible for stationary targets in which the front-wall reflections should be properly attenuated before image formation. Recently, the well-known wall mitigation techniques applicable under CS framework are spatial filtering and single-value decomposition-based approaches [30, 32].

In spatial filtering, the zero spatial frequency of the wall contribution is used as peculiar characteristic to distinguish it from the target returns. Therefore, separating wall reflection from the target returns amounts to basically separating a zero-frequency signal from non-zero frequency-valued signals across antennas, which can be easily achieved using a proper spatial filter [28, 30]. Mathematically, the spatial filter that notches out the constant component can be realized as the subtraction of the average value of the return across the
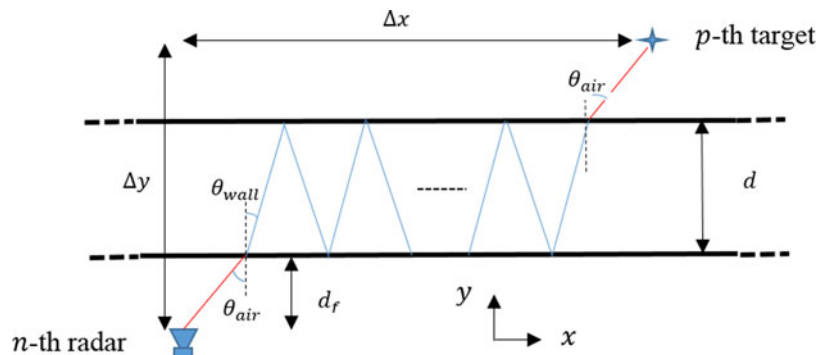

Fig. 2. Wall reverberation phenomenon.

antennas leaving the data free from front-wall clutters. The filtered signal $\tilde{y}[m, n]$ is therefore given by [30]:

$$\tilde{y}[m, n] = y[m, n] - \frac{1}{N} \sum_{n=0}^{N-1} y[m, n]. \tag{6}$$

In [30], it was shown that both spatial filtering and subspace projection methods give better results when applied under CS framework. In this work, the former technique has been adopted.

III. PROPOSED GHOST SUPPRESSION METHODS

To address the challenges on the existing ghost suppression methods, we propose multipath ghost suppression technique, which incorporates AD feature of the multipath ghosts under CS framework. The introduction of AD feature simplifies the problem in terms of complexity and relaxes the requirement of knowing the reflecting geometry. In this case, we can reconstruct the scene without the complete knowledge of the location of the reflecting geometry.

In the reconstruction process, consider (2) as a perfect reverse model. Factorizing in (2) with respect to $\Phi^{(o)}$ gives (7).

$$y = \Phi^{(o)} \Bigg[s^{(o)} + \Phi^{(o)-1} \sum_{r=1}^{R-1} \Phi^{(r)} s^{(r)} + \Phi^{(o)-1}$$

$$\sum_{r_w=0}^{R-1} \Phi_w^{(r_w)} s_w^{(r_w)} + \Phi^{(o)-1} \sum_{\substack{p, q=0 \\ p \neq q}}^{N_x N_y - 1} \sigma_q \Psi_q^{(o)} s_q^{(o)} \tag{7}$$

$$+ \ldots + \Phi^{(o)-1} \sum_{\substack{p, q=0 \\ p \neq q}}^{N_x N_y - 1} \sigma_q \Psi_q^{(R-1)} s_q^{(R-1)} \Bigg] + v.$$

If we define a residual column vector, w, which contains information from other subimages as:

$$w = \Phi^{(o)-1} \Bigg[\sum_{r=1}^{R-1} \Phi^{(r)} s^{(r)} + \sum_{r_w=0}^{R-1} \Phi_w^{(r_w)} s_w^{(r_w)} + \sum_{\substack{p, q=0 \\ p \neq q}}^{N_x N_y - 1} \sigma_q \Psi_q^{(o)} s_q^{(o)}$$

$$+ \ldots + \sum_{\substack{p, q=0 \\ p \neq q}}^{N_x N_y - 1} \sigma_q \Psi_q^{(R-1)} s_q^{(R-1)} \Bigg]. \tag{8}$$

Then (8) can be rewritten as:

$$y = \Phi^{(o)}(s^{(o)} + w) + v. \tag{9}$$

Defining the transformed subimage, $\check{s}^{(o)} = s^{(o)} + w$, then (9) becomes:

$$y = \Phi^{(o)} \check{s}^{(o)} + v. \tag{10}$$

Now, only direct path information, $\Phi^{(o)}$, is used to reconstruct the modified scene. Since the reconstructed scene contains some contributions from other multipath returns, then it is populated by ghosts. We hypothesize that by properly shifting the array, the ghost locations can exhibit significant shifts enough to identify them from genuine targets.

By making independent sets of measurements using undersampling matrices $D_i \in \{0, 1\}^{J \times MN}$ with $J \ll M$. The matrix D_i is known to obey restricted isometry property [25, 33]. The optimum length of the subaperture, lN, for a given compressed frequency set is a function of the number of targets, P and surrounding scatters, where l is the ratio of the selected radar locations. In TWRI applications, this number is unknown beforehand. However, it can be estimated prior to running the actual measurement [34].

$$J \geq CPR \log \left(\frac{N_x N_y}{PR} \right), \tag{11}$$

where C is a positive constant defined in CS literature. Downsampling (10) gives:

$$\bar{y}_i = D_i \Phi^{(o)} \check{s}_i^{(o)} + \bar{v}_i, \tag{12}$$

where $\bar{v}_i$ is the resulting noise vector. The compressed measurements, $\bar{y}_i$, are taken such that the corresponding subimages exhibit significant AD feature.

To exploit the AD feature, the given array is divided into subapertures. The images corresponding to these subapertures are sparsely reconstructed and then strategically combined to get a final image. A careful increase in the number of subarrays may increases the quality of the final image with the expense of computational cost. To overcome the challenge, we suggest duo-subaperture imaging with careful image fusion strategies to ameliorate the efficacy of the proposed method. Two random sets of locations, S_i, $i = 1, 2$, are chosen from a linear array of N locations with interelement spacing of d units as shown in Fig. 3.

$$S_1 = \left\{ x : 1 \leq x \leq \frac{N}{2} \right\}, \ S_2 = \left\{ x : \frac{N}{2} \leq x \leq N \right\}, \tag{13}$$

$$|S_1| = |S_2| = lN.$$

$|S_i|$ is the number of locations in the ith subarray and l denotes the ratio of the selected radar locations.
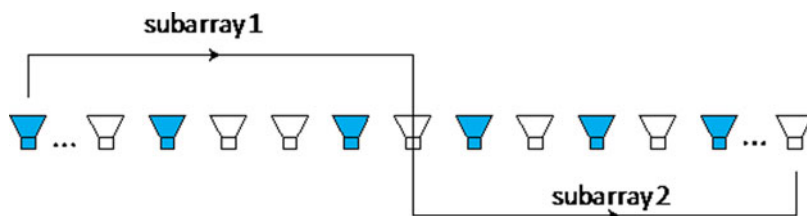

Fig. 3. Subarrays selection.

The selected subapertures (colored in blue) are then used to design the sensing matrices for image sensing and reconstruction.

A) Rationale of subarrays selection

The given array is subdivided into two halves making two subarrays with their centers separated by around $N/2$. It is desired to optimally decide the subarray separation to ensure maximum ghost suppression. To satisfy the desire, we perform correlation analysis of the received signals. Consider two observation vectors, y_n and y_{n+k}, when the subarrays are separated by kd units. It is hypothesized that the observed scenes will be different due to AD feature of the multipath contribution. From (12) we have:

$$\bar{y}_n = A_n \breve{s}_n^{(o)} + \bar{v}_n$$
$$\bar{y}_{n+k} = A_{n+k} \breve{s}_{n+k}^{(o)} + \bar{v}_{n+k}. \tag{14}$$

The correlation of the received signals, $R_{n,n+k}$ is given by $R_{n,n+k} = E\{\bar{y}_n, \bar{y}_{n+k}^H\} = A_n R_{s_n s_{n+k}} A_{n+k}^H + R_v; R_{s_n s_{n+k}} = E\{\breve{s}_n^{(o)}, \breve{s}_{n+k}^{(o)H}\}$. We need the value of k that minimizes the number of non-zero elements in $R_{s_n s_{n+k}}$. However, the matrix $A_i = D_i \Phi^{(o)}$ is a function of the time delay, which also depends on the target location and it is unknown in *priori*. Hence, developing a closed form expression for the aperture separation is not feasible.

To overcome that challenge, a fairly exhaustive search of the acceptable subarray separation was conducted for random target locations placed in a room of 5×5 m². Array of 2 m long and 77 locations, which conforms to most TWRI applications, was deployed. In each run, a different target location was assumed and their corresponding images were captured. The subarray was then linearly shifted along the cross-range direction and determine the cross-correlation between the current image vector, s_k and the initial image, s_o. The normalized correlation value is given by:

$$R_k = \frac{s_k^H s_o}{|s_k||s_o|}. \tag{15}$$

The effective separation is determined when there is no significant change on the cross-correlation of the two images. The sample representation of the results for different target locations is shown in Fig. 4 where only five are displayed for clarity.

It can be concluded from Fig. 4 that the AD effect is more pronounced when the target is closer to the radar as the normalized correlation converges to a constant value after fewer subarray shifts. It is evident from Fig. 4(b) that the separation of $N/2$ may suffice. In other words, for all randomly selected target locations, the value of the correlation converges nearly to the same value after $N/2$, where N signifies the number of radar locations. We repeated the experiment using different room dimensions and we arrived at similar conclusions. The selected subarrays are then used to design the sensing matrices for image sensing and reconstruction.

B) Sensing matrix design and analysis

In TWRI, the sensing matrix can be viewed as the product of two matrices. The first is a predefined matrix describing the signal propagation model in (2), which is a function of the radar parameters and reflecting geometry. The second matrix is downsampling matrix, D, which compresses the data based on CS theories. Therefore, designing the sensing matrix in TWRI basically is designing the matrix D. The matrix D in this work consists of randomly chosen rows from an identity matrix as in [3, 4, 35]. In stepped frequency radar, the downsampling occurs in the frequency and radar locations.

In CS theory, the sensing matrix plays an important role in the signal reconstruction process. To ensure the recoverability of the signal, the columns of the sensing matrix, $A_i = D_i \Phi^{(o)}$, should have low correlation.

To analyze the recoverability of the sensing matrices, we evaluate the mutual coherence of the sensing matrix. The mutual coherence of the two columns is the normalized inner product between them, while the coherence of the matrix is the maximum absolute value of this inner product among all pairs of elements in the matrix [34, 36]:

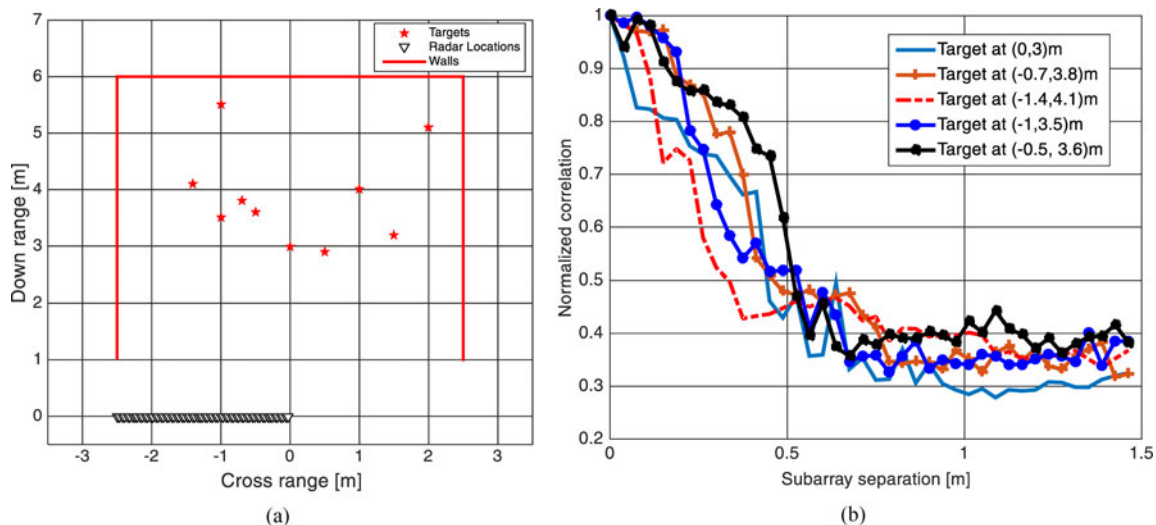$$\mu(A) = \max_{i \neq j} \frac{|a_i^H a_j|}{a_i a_j}. \tag{16}$$

Fig. 4. (a) Scene with 10 random targets, (b) normalized correlation for five targets.

Measurement (%)	Full array		Subarray	
	32×32	64×64	32×32	64×64
6	0.469	0.812	0.783	0.941
12	0.432	0.802	0.786	0.945
25	0.418	0.795	0.782	0.941

When this metric returns a small value, it serves as sufficient condition to ensure sparse reconstruction. In classical algorithms, it may also provide useful information on the performance of the array including resolution, noise, and other interference robustness and ambiguity [37].

The mutual coherence of the sensing matrix for various undersampling ratios and two image resolutions, averaged over 100 Monte-Carlo runs, are summarized in Table 1. The duo-subarray-based sensing matrix is compared with normal array sensing matrix. It is observed that the coherence increases with the image resolution. For subarray configuration discussed, the mutual coherence shows no significant change with data volume.

Though, the coherence of the matrix is relatively high, but the mutual coherence is only a sufficient but not necessary condition to ensure perfect reconstruction. Using simulated and experimental data, we attained a very good image quality with similar measurement matrices.

Figure 5(a) shows a normalized correlation of the representative column for image resolution of 32×32 pixels, and Fig. 5(b) shows a correlation of a representative column for image resolution of 64×64 pixels when the undersampling ratio is 6%. The selected columns are column 500 for the case of 32×32 pixels and 2000 for the case of 64×64 pixels.

C) Subimages sparse reconstruction

The modified subimage, $\check{s}_i^{(o)}$, in (12) can be reconstructed sequentially using conventional CS approach [38, 39] or concurrently to speed up the reconstruction process.

The reconstructed vectors, $\check{s}_i^{(o)}$, are obtained by solving optimization problem [38, 39]:

$$\widetilde{\check{s}_i^{(o)}} = \underset{\check{s}_i^{(o)}}{\arg\min} \ \|\check{s}_i^{(o)}\|_1$$

$$\text{s.t.} \quad \|\bar{y}_i - D_i \Phi^{(o)} \check{s}_i^{(o)}\|_2 < \varepsilon. \tag{17}$$

The choice of ε is a function of noise power [40]. To eliminate the effect of the ghosts exploiting AD feature, the reconstructed subimages are strategically fused to yield a final image.

D) Image fusion strategies

When multiple and distinct compressed subapertures are considered as in Fig. 3, then the resulting ghosts in the respective subimages will be positioned differently following ghost AD feature. However, the true targets maintain the same location in all images. Therefore, a strategic fusion of the subimages is needed to suppress the effect of multipath ghosts.

The overall image is obtained by masking which involves pixel-wise multiplication of the individual subimages [16, 18, 26].

Suppose there are L subimages, with s_{lp} defines the image value at the pth pixel corresponding to the lth subimage, the overall image is obtained as:

$$s(p) = \prod_{l=1}^{L} \check{s}_{lp}^{(o)} \tag{18}$$

Masking sometimes tends to suppress the genuine targets or enhances the residual clutters [19]. In this work, we propose strategic image fusions, additive–multiplicative fusions, which can reduce this effect. In additive–multiplicative fusion, an intermediate image is first obtained as the strategic summation of the individual subimages. The summation is taken such that the magnitude of the true targets is preserved while minimizing the clutters. This helps to reduce the effect of the ghost and other clutters and hence increase target relative clutter peak (TRCP) at target locations. The intermediate image is then masked with the subimages to obtain the final image. We propose two subimage fusion strategies to enhance the image quality.
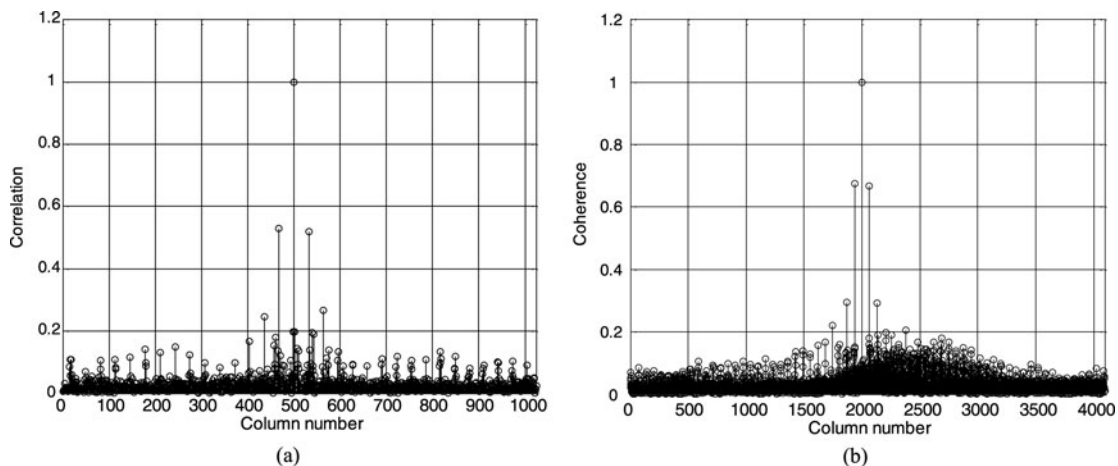

Fig. 5. Sample of normalized correlation of the proposed sensing matrix: (a) 500th column for 32×32 pixels, (b) 2000th column for 64×64 pixels.

1) WEIGHTED SUM-BASED
ADDITIVE−MULTIPLICATIVE FUSION (WSAM)

In this case, the intermediate image is the weighted sum, which minimizes the l_2 norm while maintaining the magnitudes of the true targets. Consider L subimages, $\check{s}_1^{(o)}$, $\check{s}_2^{(o)} \ldots \check{s}_L^{(o)}$, reconstructed from L compressed apertures. Their weighted mean is given by:

$$s_W(p) = \sum_l^L \alpha_l \check{s}_l^{(o)}(p), \qquad (19)$$

where $\alpha_l \in \mathbb{R} : 0 \leq \alpha_l \leq 1$. The values of α_l, which result in a minimum norm, are obtained using:

$$\min \| \alpha_1 \check{s}_1^{(o)} + \ldots + \alpha_L \check{s}_L^{(o)} \| \text{ subject to } \sum_{l=1}^L \alpha_l = 1. \qquad (20)$$

2) HARMONIC MEAN-BASED
ADDITIVE−MULTIPLICATIVE FUSION (HMAM)

The fact that harmonic mean of a list of non-negative numbers leans towards the least elements of the list while maintain the same value for equal elements can be utilized to suppress large clutters in TWRI while it maintains the true targets. For L subimages, $\check{s}_1^{(o)}$, $\check{s}_2^{(o)} \ldots \check{s}_L^{(o)}$, reconstructed from L compressed subaperture, the intermediate image, s_H, is defined as the harmonic mean of the corresponding subimages and is given by:

$$s_H(p) = \frac{L}{\sum_{l=1}^L (1/\check{s}_l^{(o)}(p))}. \qquad (21)$$

The overall image is obtained by masking the intermediate image with subimages.

For comparison, conventional delay and sum beamforming (DSBF) is used for image reconstruction. Given a set of measurements collected from N different transceiver locations with M monochromatic frequencies transmitted at every radar position. The complex image $I(x_p, y_p)$ of the pth grid point (x_p, y_p) is obtained by summing phase-shifted copies of the available signals [8, 24]:

$$I(x_p, y_p) = \frac{1}{MN} \sum_{n=0}^{N-1} \sum_{m=0}^{M-1} y[m, n] \exp(j2\pi f_m \tau_{pn}), \qquad (22)$$

where τ_{pn} is the focusing delay for the nth transceiver and the pth grid point.

IV.   RESULTS AND DISCUSSION

A) Simulation results

A TWRI system was simulated using MATLAB®. For comparison, we adopt simulation parameters and setup as in [8]. The left- and right-side walls of the room are at cross-range of −1.8 m and 4 m, respectively, while the back wall resides at 6.37 m downrange. A SAR, which simulates a uniform linear monostatic array composed of 77 elements spaced out by 1.9 cm is used to capture the image. The center of the array is

taken to be the origin of the system. The front wall parallel to the array is at 2.44 m downrange with thickness $d = 20$ cm and relative permittivity $\varepsilon_r = 7.67$. A series of 201 monochromatic waves to realize a UWB signal occupying a spectrum between 1 and 3 GHz is employed for the scene interrogation.

The image of the scene was reconstructed with and without the front-wall mitigation. In this work, we define a path from the radar to the target or vice versa as partial path. A total of six multipath returns were considered in this work, where one partial path is always the direct path and the second partial path corresponds to: direct, back-wall multipath, left-side, right-side wall, and the wall reverberation multipath. A return due to the target interaction was also taken into account. We assume all side walls as perfect reflectors. When they are not perfect reflectors, then ghost targets will have less power, and hence, becomes relatively easy to be suppressed. During simulation, targets located at (0.31, 3.6) and (−0.62, 5.2) m were considered. White noise of 0 dB SNR was added to the simulated measurements. The DSBF image utilizing full available measurement is obtained for comparison. For the CS reconstructions, we use only 10% of the total measurement to reconstruct the corresponding images using Yall1 algorithm [41].

The given array is divided into two halves, duo-subarray, to realize the AD effect of the resulting ghosts and then a fraction of the radar positions and frequency bins are selected from the two subarrays for sparse image reconstruction. We examine four different scenarios to evaluate the effectiveness of the proposed method under different data collocation modalities.

1) SCENARIO 1: WHOLE SUBARRAYS

In this case, we used only one-fifth of the frequency randomly selected and the same set is transmitted at each location of the given subarray. The radar locations represent one-half of the total available locations, which makes the compressed measurement 10% of the total data volume. The scene's layout and setup of this scenario is shown in Fig. 6.

The subarray images are depicted in Fig. 7. The image quality using CS reconstruction is better than DSBF in spite of using entire measurement set. To obtain the final images,
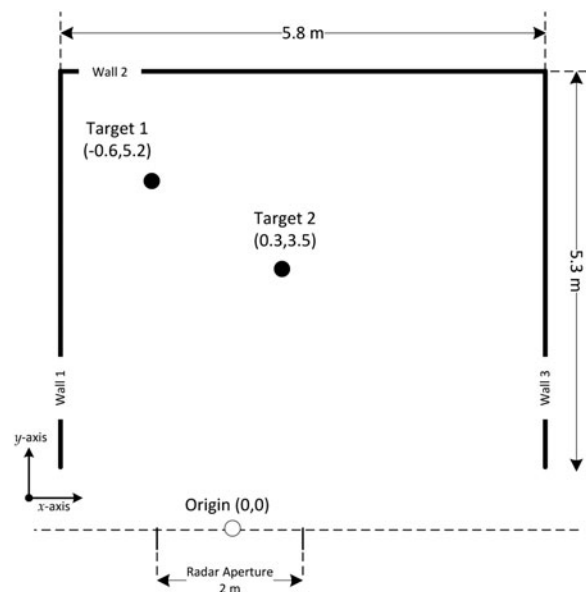

Fig. 6. Scene's layout for scenario 1.

the two subimages were combined using proposed image combining techniques: WSAM fusion and HMAM fusion and are shown in Figs 7(d)–(f). Figure 7(d) is the final image using conventional masking for performance comparison. It is evident from Fig. 7 that the proposed fusion strategies perform better than conventional masking.

In the case of WSAM fusion, the intermediate image takes 54 and 46% of the intensity of first and second subimage, respectively, to minimize the clutter norm while maintaining the intensities of the true targets. The proposed image fusion techniques seem to have comparable performance and since the WSAM ensures the minimum clutter norm compared with HMAM, it is therefore preferred in practice and will be used to evaluate the final images in the coming scenarios.

To analyze the power of sparse reconstruction over DSBF algorithm, we generated DSBF images with the same reduced data volume as shown in Figs 7(g)–(i). Apparently from Fig. 7(i), DSBF showed inability to incorporate the AD feature for ghost suppression under reduced measurement scenario owing to its lower resolution caused by point spread function. Further, it suffers from increased level of unwanted clutters due to the violation on the required antenna spacing, and therefore, will not be compared in the proceeding results.

Using quantitative measures, we evaluated target signal-to-clutter ratio (TSCR) and TRCP and are summarized in Table 2.

From Table 2 and Fig. 11(a), the method can dramatically attenuate the effect of the multipath ghosts. Only a threshold value of around 30% of the maximum can be used to isolate true targets from the surrounding clutters.

For target detection capability, the precisions of this scenario are demonstrated in Fig. 11(a). The precision metric used is defined as the ratio of the true positives "genuine targets" to the sum of the true positives and the false positives "false alarms", where the false positives are the ghosts. Precision can be expressed by

$$\text{Precision} = \frac{TP}{TP + FP}. \quad (23)$$

If there is no ghost for a given threshold value, the value of precision becomes unity. The metric will continue working even for extended targets.
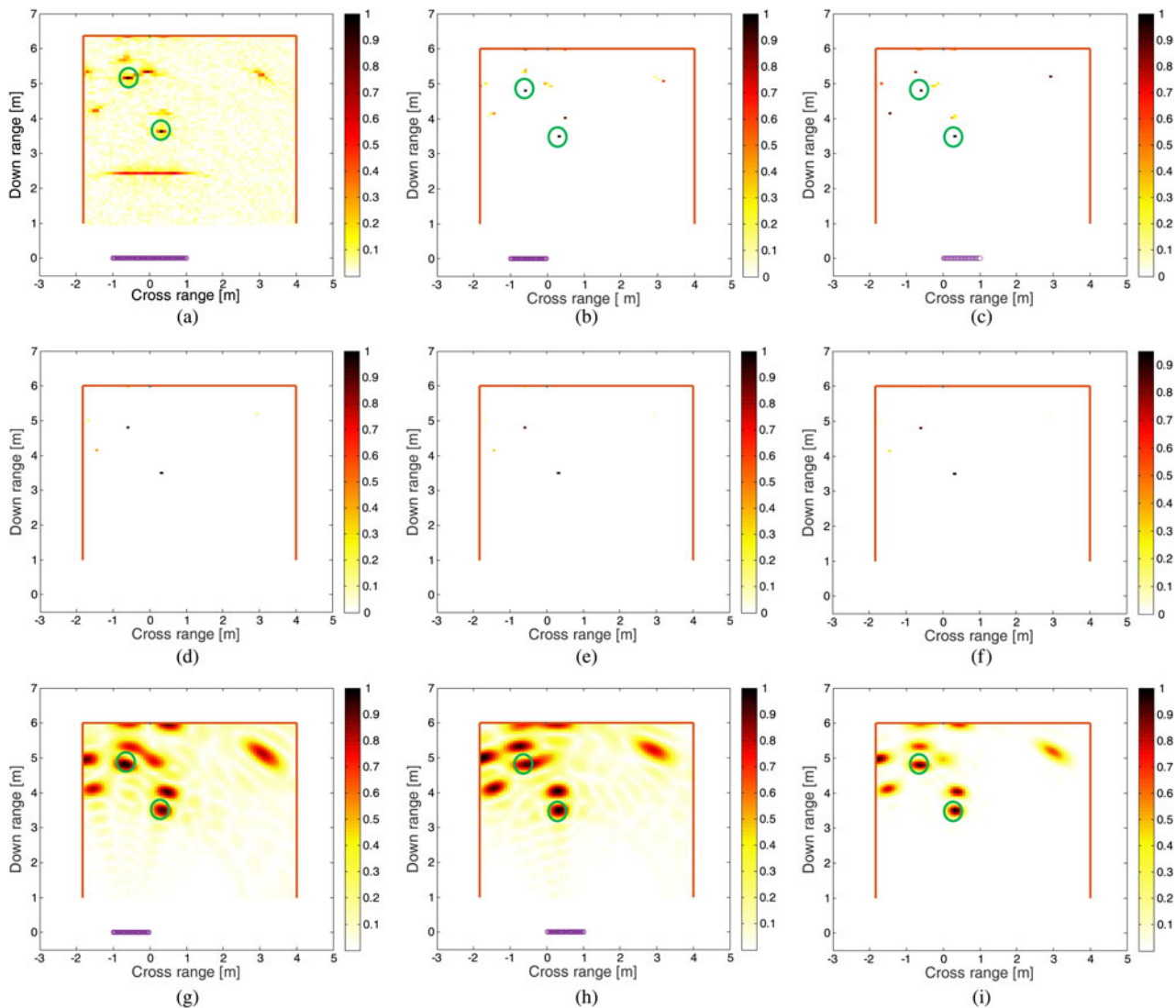

Fig. 7. Images with random frequency: (a) DSBF with full data, (b) subarray 1, (c) subarray 2, (d) final with masking, (e) final with WSAM 54% by 46%, (f) final with HMAM, (g) subarray 1 DSBF, (h) subarray 2 DSBF, and (i) final DSBF.

Table 2. TSCR and TRCP for whole subarrays.

	TSCR	TRCP
Initial image	57.4	0.8
Masking	72.3	6.7
WSAM	76.5	9.7
HMAM	78.0	10.5

Table 3. TSCR and TRCP for different scenarios.

	Scenario 2		Scenario 3		Real data	
	TSCR	TSCR	TSCR	TSCR	TSCR	TSCR
Initial image	57.7	1.0	62.7	2.0	57.5	2.6
Masking	72.4	6.7	89.5	16.9	77.6	10.9
WSAM	76.7	10.1	97.3	23.7	88.0	20.2

2) SCENARIO 2: COMPRESSED SUBAPERTURES

One-half of the frequency bins were randomly chosen and the same set is transmitted at each selected location for design simplicity, and one-fifth of the radar locations were randomly selected from the given subarrays. The subaperture images are depicted in Figs 8(a) and 8(b), and their corresponding final image generated with WSAM fusion is depicted in Fig. 8(c). In WSAM, the fusion assumes 58% of the first subimage and 42% of the first second to effectively suppress the ghosts. In Fig. 8, the final image suppresses the multipath ghosts significantly and genuine targets can be detected. This observation is supported by numerical analysis using TSCR and TRCP, which show relatively good values enough to detect the targets as summarized in Table 3.

The precision curves, which dictate the probability of correct detection, are plotted against the threshold values are shown in Fig. 11(b). The threshold of around 35% can correctly eradicate the surrounding clutters including ghosts.

3) SCENARIO 3: COMPRESSED SUBAPERTURES WITH SINGLE-VIEW BISTATIC CONFIGURATION

In the above setups, we considered monostatic radar system: transmitter and receiver are collocated. In this setup, we investigate the effect of bistatic radar configuration. The transmitter's location is fixed at the center of the array, then two receiver locations are selected randomly. The corresponding subimages are shown in Figs 9(a) and 9(b), and the corresponding final image with WSAM is depicted in Fig. 9(c) with its quality metrics summarized in Table 3.

The precision curves, which compare the number of true targets and the total number of available targets, are shown in Fig. 11(c). It is noted in Fig. 11(c) that the threshold of 15% suffices as detection threshold. This scenario shows a noticeable increase in the image quality compared with 35% threshold of its corresponding multi-view monostatic counterpart.

4) SCENARIO 4: SINGLE-VIEW BISTATIC WITH FRONT WALL

Using duo-subaperture, we can reconstruct the image without the need to mitigate the front wall. Applying the discussed fusion strategies, we can suppress the effect of the front wall, provided the measurement volume is adequate as recommended by the CS algorithms. The final image restores the
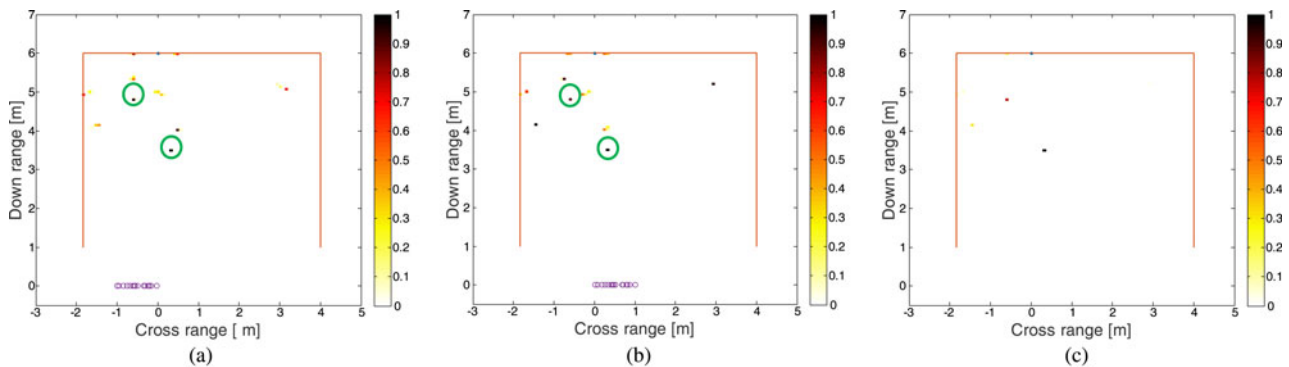
Fig. 8. Images: (a) subarray 1, (b) subarray 2, and (c) final with WSAM 58% by 42%.
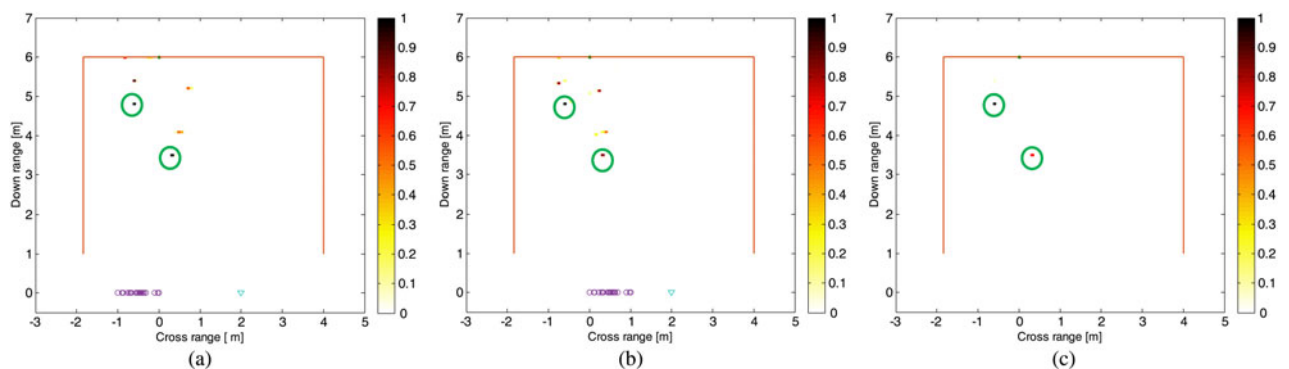
Fig. 9. Images for single-view bistatic: (a) subarray 1, (b) subarray 2, and (c) final with WSAM 44% by 56%.
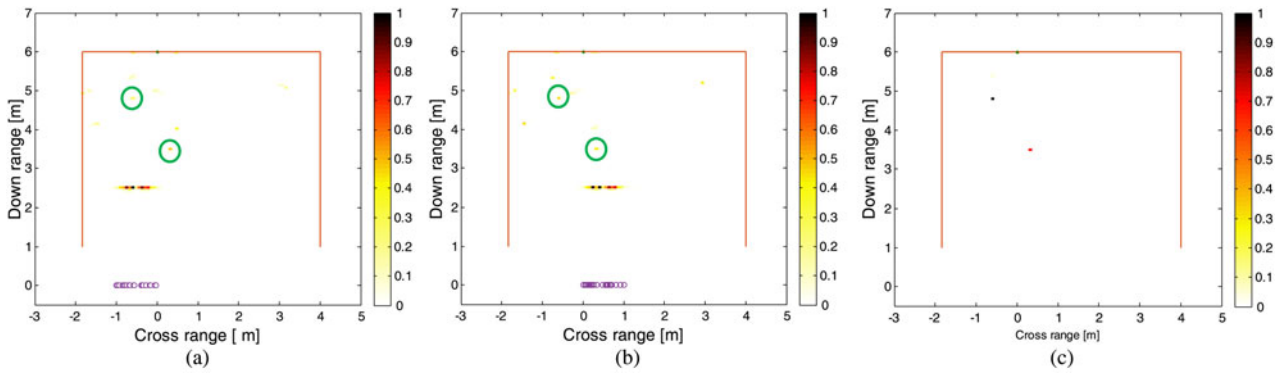
Fig. 10. Image reconstruction with front wall: (a) subaperture 1, (b) subaperture 2, and (c) final with WSAM.

intensities of the true targets and the wall is masked out as shown in Fig. 10.

The precision in Fig. 11(d) demonstrates the effectiveness of the method even with front wall at the expense of increasing measurement volume as the scene becomes less sparse. With WSAM fusion, no postprocessing is needed to identify the true target as the ghosts are highly attenuated.

It should be pointed out that the target size will affect the aspect dependency and hence the suppression accuracy.

B) Experimental results

A wideband SAR system was set up in a semicontrolled room at KFUPM-EE department for multipath analysis to validate the proposed ghost suppression method; a schematic sketch of the room as shown in Fig. 12. The SAR was deployed to cover 67 equally spaced locations with an interelement spacing of 2.5 cm along the X-axis. A stepped frequency signal occupying a spectrum between 1 and 3 GHz with 801 frequency points was used for scene interrogation. The
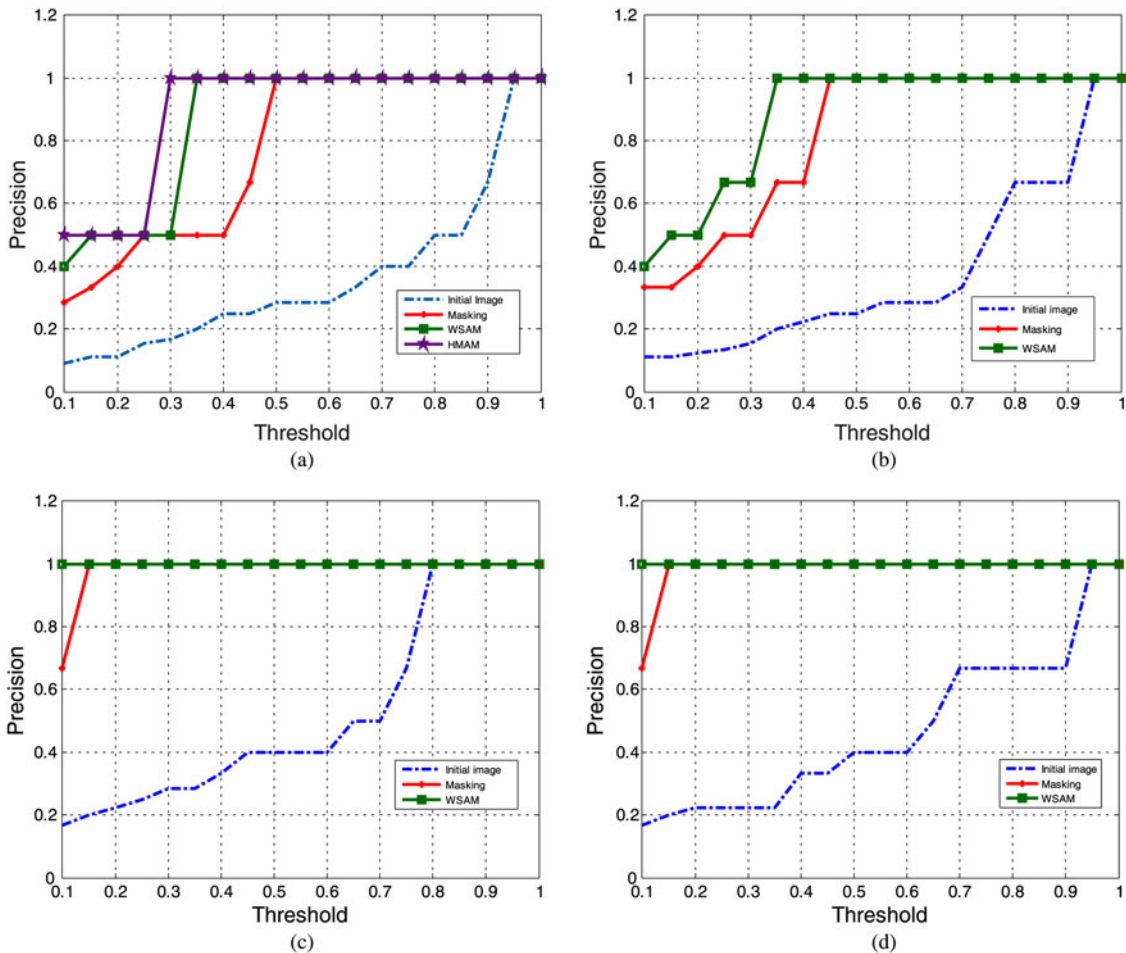

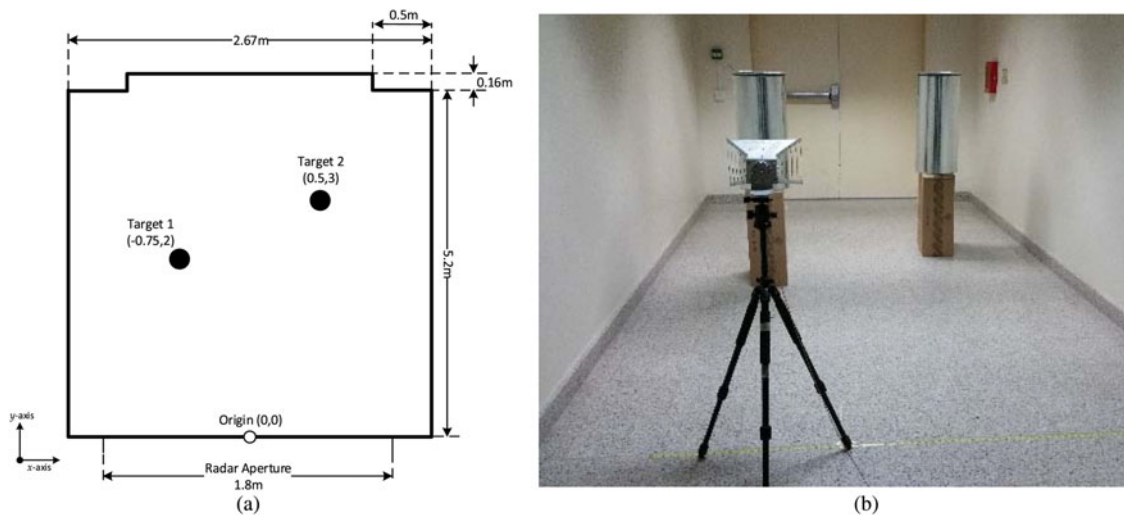**Fig. 11.** Precision curves: (a) scenario 1, (b) scenario 2, (c) scenario 3, and (d) scenario 4.

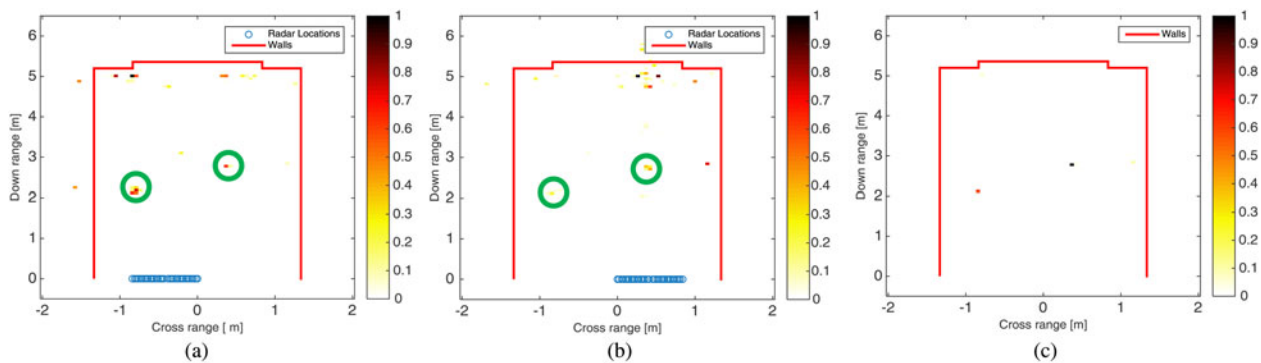**Fig. 12.** (a) The setup and room layout, (b) photograph of the scene setup.

Fig. 13. Images: (a) subaperture 1, (b) subaperture 2, and (c) final with WSAM.

background information was first captured for clutter suppression. Two metallic cylinders were placed at $(-0.75, 2)$ and $(0.5, 3)$ m as shown in the setup and room layout given by Fig. 12 with the origin taken at the center of the aperture. The room has two protruding corners of reinforced concrete pillars near the back side. The imaged region is chosen to be 4×5 m².

To identify and suppress multipath ghosts, duo-subaperture with one-third of the radar locations are randomly selected and only one-eighth of the frequency bins were transmitted. Figures 12(a) and 12(b) show the images of selection of the duo-subaperture. The final image is obtained using WSAM fusion, which shows significant ghost reduction with all true targets correctly reconstructed despite the directivity challenge of the horn antenna as shown in Figs 13(a) and 13(b). This observation alludes that in real application, the subaperture need to be carefully chosen; otherwise, some real targets might be invisible by the radar system.

Quantitative performance measures, TSCR and TRCP defined in [1] summarized in Table 3, indicate the effectiveness of the suppression method.

The variation of the precision value with the possible threshold is given in the precision curves in Fig. 14, which indicates that the targets can be correctly detected without additional postprocessing.

Comparison with related works

Comparing with recent works, our method shows satisfactory tradeoff between image quality improvement and complexity reduction. In [18], the authors achieved optimal tradeoff between improvement factor (IF) of 24.29 dB and target improvement factor (TIF) of 0.29 dB when using single-view multistatic radar with multiplicative–additive fusion of seven
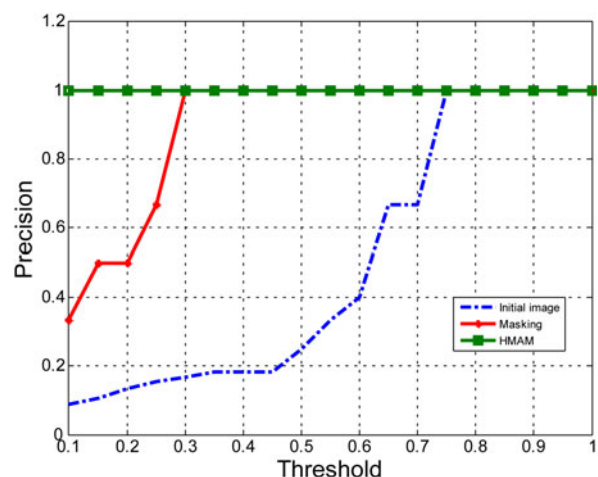

Fig. 14. Precision curves under real data.

subarray images. The limited performance is due to point spread function in DSBF algorithm, which significantly lowers its resolution. In addition, the DSBF images suffer from increased level of unwanted clutters. In this work, we employed compressed duo-subaperture under CS framework and achieved 34.6 dB of IF and 21.7 dB of the TIF. Moreover, unlike in [18] where the authors tackled only multipath ghosts due to target interactions, this work considered multipath due to side-wall and front-wall reverberation as well.

In [8], the presented method achieved the best suppression when using non-overlapping group sparse approach. It returned TSCR of 95 dB and TRCP of 25 dB with around 3% of the total measurement. Using nearly equal volume, the proposed method achieves TSCR of 97.3 dB and TRCP of 23.7 dB with WSAM image fusion strategy. In addition to front-wall and side-wall reflection considered in [8], the work incorporated target-to-target interaction as well, which gives additional credit.

V. CONCLUSIONS

This paper proposed efficient multipath ghost suppression technique in TWRI exploiting the AD characteristic of the multipath ghosts under CS framework without the knowledge of the scene geometry. The method was scrutinized for different data collection modalities to evaluate its efficacy. New sub-images combining strategies were proposed, which improves the TSCR at target locations. Further, two antenna deployments were studied using multiview monostatic and single-view bistatic configurations. The latter showed better results in both TSCR and TRCP, which increases the probability of correct detection.

As the extension of this work, the optimum subarrays separation can be investigated to ensure sufficient ghost suppression. Further, the proposed method is effective for pixel-sized targets; more analysis is required for extended targets scenarios (target occupying more than one pixel).

ACKNOWLEDGEMENTS

REFERENCES

[1] Abdalla, A.T.; Muqaibel, A.H.; Al-Dharrab, S.: Aspect dependent multipath ghost suppression in TWRI under compressive sensing framework, in 2015 Int. Conf. Communications, Signal Processing, and their Applications (ICCSPA), Sharjah, 2015, 1–6.

[2] Abdalla, A.T.; Muqaibel, A.H.: Multiple target sparse reconstruction in TWRI utilizing ghost's aspect dependence feature, in 2015 IEEE International RF and Microwave Conf. (RFM), Kuching, 2015, 280–284.

[3] Amin, M.G.; Ahmad, F.: Compressive sensing for through-the-wall radar imaging. J. Electron. Imaging, **22** (3) (2013), 30901.

[4] Amin, M.G.: Through-the-Wall Radar Imaging, CRC Press, Taylor and Francis Group, New York, 2010.

[5] Baranoski, E.J.: Through wall imaging: historical perspective and future directions, 2008 IEEE Int. Conf. Acoustics, Speech and Signal Processing, Las Vegas, NV, 2008, 5173–5176.

[6] Burchett, H.: Advances in through wall radar for search, rescue and security applications, in Proc. Institute of Engineering and Technology Conf. Crime and Security, London, UK, 2006, 511–525.

[7] Charvat, G.L.; Kempel, L.C.; Rothwell, E.J.; Coleman, C.M.; Mokole, E.L.: A through-dielectric radar imaging system. IEEE Trans. Antennas Propag., **58** (8) (2010), 2594–2603.

[8] Leigsnering, M.; Ahmad, F.; Amin, M.; Zoubir, A.: Multipath exploitation in through-the-wall radar imaging using sparse reconstruction, *IEEE Trans.* Aerosp. Electron. Syst., **50** (2) (2014), 920–939.

[9] Setlur, P.; Alli, G.; Nuzzo, L.: Multipath exploitation in through-wall radar imaging via point spread functions. IEEE Trans. Image Process., **22** (12) (2013), 4571–4586.

[10] Chakraborty, B.; Li, Y.; Zhang, J.J.; Trueblood, T.; Papandreou-Suppappola, A.; Morrell, D.: Multipath exploitation with adaptive waveform design for tracking in urban terrain, in 2010 IEEE Int. Conf. Acoustics, Speech and Signal Processing, Dallas, TX, 2010, 3894–3897.

[11] Linnehan, R.; Schindler, J.: Multistatic scattering from moving targets in multipath environments, in 2009 IEEE Radar Conf., Pasadena, CA, 2009, 1–6.

[12] Krolik, J.L.; Farrell, J.; Steinhardt, A.: Exploiting multipath propagation for GMTI in urban environments, in IEEE Conf. on Radar, New York, USA, 2006, 4–9.

[13] Yoon, Y.-S.; Amin, M.: Compressed sensing technique for high resolution radar imaging, Proc. SPIE Signal Processing Sensor Fusion Target Recognition. XVII, 2008, 69681A-69681A-10.

[14] Setlur, P.; Amin, M.; Ahmad, F.; Member, S.: Multipath model and exploitation in through-the-wall and urban radar sensing. IEEE Trans. Geosci. Remote Sens., **49** (10) (2011), 4021–4034.

[15] Tan, Q.: A new method for multipath interference suppression in through-the-wall UWB radar imaging, in 2nd Int. Conf. on Advanced Computer Control, Shenyang China, 2010, 535–540.

[16] Li, Z.; Kong, L.; Jia, Y.; Zhao, Z.; Lan, F.: A novel approach of multipath suppression based on sub-aperture imaging in through-wall-radar imaging, in 2013 IEEE Radar Conf. (RadarCon13), Ottawa, ON, 2013, 1–4.

[17] Tan, Q.; Leung, H.; Song, Y.; Wang, T.: Multipath ghost suppression for through-the-wall radar. IEEE Trans. Aerosp. Electron. Syst., **50** (3) (2014), 2284–2292.

[18] Gennarelli, G.; Soldovieri, F.: Multipath ghosts in radar imaging: physical insight and mitigation strategies. IEEE J. Sel. Top. Appl. Earth Obs. Remote Sens., **8** (3) (2015), 1078–1086.

[19] Yan, D.; Cui, G.; Guo, S.; Kong, L.; Yang, X.; Liu, T.: Multipath ghosts location and sub-aperture based suppression algorithm for TWIR, in 2016 IEEE Radar Conf. (RadarConf), Philadelphia, PA, 2016, 1–4.

[20] Chen, X.; Chen, W.: Multipath ghost elimination for through-wall radar imaging. IET Radar Sonar Navig., **10** (2) (2016), 299–310.

[21] Leigsnering, M.; Ahmad, F.; Amin, M.G.; Zoubir, A.M.: Compressive sensing based specular multipath exploitation for through-the-wall radar imaging, in 2013 IEEE Int. Conf. Acoustics, Speech and Signal Processing, Vancouver, BC, 2013, 6004–6008.

[22] Wang, J.; Wang, P.; Li, Y.; Song, Q.; Zhou, Z.: A multipath suppression technique for through-the-wall radar, in 2013 IEEE Int. Conf. on Ultra-Wideband (ICUWB), Ieee, 2013, 215–220.

[23] Ralston, T.S.; Charvat, G.L.; Peabody, J.E.: Real-time through-wall imaging using an ultrawideband multiple-input multiple-output (MIMO) phased array radar system, in 2010 IEEE Int. Symp. on Phased Array Systems and Technology, Waltham, MA, 2010, 551–558.

[24] Ahmed, F.; Amin, M.G.; Kassam, S.: A beamforming approach to stepped-frequency synthetic aperture through-the-wall radar imaging, in Proc. of the IEEE First Int. Workshop on Computational Advances in Multi-Sensor Adaptive Processing, Puerto Vallarta, Mexico, 2005, 24–27.

[25] Gurbuz, A.C.; McClellan, J.H.; Scott, W.R.: A compressive sensing data acquisition and imaging method for stepped frequency GPRs. IEEE Trans. Signal Process., 57 (7) (2009), 2640–2650.

[26] Setlur, P.; Amin, M.; Ahmad, F.: Multipath model and exploitation in through-the-wall and urban radar sensing. IEEE Trans. Geosci. Remote Sens., 49 (10) (2011), 4021–4034.

[27] Karousos, A.; Koutitas, G.; Tzaras, C.: Transmission and reflection coefficients in time-domain for a dielectric slab for UWB signals, in VTC Spring 2008 – IEEE Vehicular Technology Conf., Singapore, 2008, 455–458.

[28] Yoon, Y.-S.; Amin, M.: Spatial filtering for wall-clutter mitigation in through-the-wall radar imaging. IEEE Trans. Geosci. Remote Sens., 47 (9) (2009), 3192–3208.

[29] Tivive, F.H.C.; Amin, M.G.; Bouzerdoum, A.: Wall clutter mitigation based on Eigen-analysis in through-the-wall radar imaging, in 2011 17th Int. Conf. Digital Signal Processing (DSP), Corfu, 2011, 1–8.

[30] Lagunas, E.; Amin, M.G.; Ahmad, F.; Nájar, M.: Wall mitigation techniques for indoor sensing within the compressive sensing framework. IEEE Trans. Geosci. Remote Sens., 51 (2) (2013), 891–906.

[31] Leigsnering, M.; Amin, M.G.; Ahmad, F.; Zoubir, A.M.: Multipath exploitation and suppression for SAR imaging of building interiors [an overview of recent advances]. IEEE Signal Process. Mag., 31 (4) (2014), 110–119.

[32] Tivive, F.; Bouzerdoum, A.; Moeness, A.: A subspace projection approach for wall clutter mitigation in through-the-wall radar Imaging. IEEE Trans. Geosci. Remote Sens., 53 (4) (2015), 2108–2122.

[33] Amin, M.; Ahmad, F.; Zhang, W.: A compressive sensing approach to moving target indication for urban sensing, in 2011 IEEE RadarCon (RADAR), Ieee, 2011, 509–512.

[34] Donoho, D.L.; Tsaig, Y.; Drori, I.; Starck, J.L.: Sparse solution of underdetermined systems of linear equations by stage wise orthogonal matching pursuit. IEEE Trans. Inf. Theory, 58 (2) (2012), 1094–1121.

[35] Leigsnering, M.: Sparsity-Based Multipath Exploitation for Through-the-Wall Radar Imaging. Technische Universität, Darmstadt, Ph.D. Thesis, 2015.

[36] Li, L.; Boufounos, P.; Liu, D.; Mansour, H.; Sahinoglu, S.: Sparse MIMO architectures for through-the-wall imaging, in 2014 IEEE 8th Sensor Array and Multichannel Signal Processing Workshop (SAM), A Coruna, 2014, 513–516.

[37] Vaidyanathan, P.P.; Pal, P.: Sparse sensing with coprime arrays. Conf. Rec. – Asilomar Conf. Signals Syst. Comput., 59 (2) (2010), 1405–1409.

[38] Donoho, D.L.: Compressed sensing. IEEE Trans. Inf. Theory, 52 (4) (2006), 1289–1306.

[39] Candès, E.J.: Compressive sampling, in Proc. of the Int. Congress of Mathematicians, Eur. Mathematical Society, Madrid, Spain (2006).

[40] Huang, Q.; Qu, L.; Wu, B.; Fang, G.: UWB through-wall imaging based on compressive sensing. IEEE Trans. Geosci. Remote Sens., 48 (2010), (3 PART2), 1408–1415.

[41] Yang, J.; Zhang, Y.: Alternating direction algorithms for L1-problems in compressive sensing. SIAM J. Sci. Comput., 33 (1–2) (2011), 250–278.

Ali Hussein Muqaibel received the B.Sc. and M.Sc. degrees from King Fahd University of Petroleum and Minerals (KFUPM), Dhahran, Saudi Arabia, in 1996 and 1999, respectively, and the Ph.D. degree from Virginia Polytechnic Institute and State University (Virginia Tech), Blacksburg, in 2003. During his study at Virginia Tech, he was with both the Time Domain and RF Measurements Laboratory and the Mobile and Portable Radio Research Group. He is currently the Director of the Telecommunications Research Laboratory (TRL) and an Associate Professor with the Electrical Engineering Department, KFUPM. His main area of interest includes ultra-wideband (UWB) signal processing for localization and communications. He was a Visiting Scholar at both Georgia Institute of Technology, Georgia, USA and Villanova University, Villanova, Pennsylvania, USA. He is the author of two book chapters and more than 90 articles. Dr. Muqaibel received many awards in the excellence in teaching, advising, and instructional technology.

Abdi Talib Abdalla received the B.Sc. degree in Electronic Science and Communication and M.Sc. degree in Electronics Engineering and Information Technology from the University of Dar es Salaam, Tanzania, in 2006 and 2010, respectively, and the Ph.D. degree from King Fahd University of Petroleum and Minerals (KFUPM), Saudi Arabia, in 2016. Currently, he is a Lecturer at the Department of Electronics and Telecommunication Engineering of University of Dar es Salaam, Tanzania. His research interests include target localization, sparse arrays processing, through-the-wall radar imaging, and application of compressive sensing to radar signal processing.

Mohammad Tamim Alkhodary received his B.S. degree in Communication Engineering from the University of Science and Technology, Sana'a, Yemen, in 2008. He received his M.S. in Telecommunication Engineering in 2011 from KFUPM. He joined the Electrical Engineering Department at KFUPM as a Lecturer in 2012, and he is now working toward his Ph.D. degree in the Department of Electrical Engineering at the same institute. In 2015, he joined KAUST for 1-year research internship. His research

interests include signal processing, UWB communication, compressive sensing theory and applications.

Suhail Al-Dharrab received his B.Sc. degree in Electrical Engineering from King Fahd University of Petroleum and Minerals, Dhahran, Saudi Arabia in 2005. He received the M.A.Sc. and Ph.D. degrees in Electrical and Computer Engineering from University of Waterloo, Waterloo, Canada, in 2009 and 2013, respectively. From 2005 to 2007, he worked as a Graduate Assistant in the Electrical Engineering Department at King Fahd University of Petroleum and Minerals. In 2015, he was a Visiting Scholar in the School of Electrical and Computer Engineering at the Georgia Institute of Technology, Atlanta, USA. He is currently an Assistant Professor in the Electrical Engineering Department and Assistant Director of the Center for Energy and Geo-Processing at King Fahd University of Petroleum and Minerals, Dhahran, Saudi Arabia. His research interests span topics in the areas of wireless communication systems, underwater acoustic communication, digital signal processing, and information theory.